Hyperbolic metamaterials for high-efficiency generation of circularly polarized Airy beams*

Lin Chen(陈林)†, Huihui Li(李会会), Weiming Hao(郝玮鸣), Xiang Yin(殷祥), and Jian Wang(王健)

Wuhan National Laboratory for Optoelectronics, Huazhong University of Science and Technology, Wuhan 430074, *China*

(Received 29 February 2020; revised manuscript received 23 April 2020; accepted manuscript online 27 May 2020)

Metasurfaces have exhibited considerable capability for generating Airy beams. However, the available plasmonic/dielectric metasurfaces Airy-beam generators have low transmission efficiency and/or poor quality of generated beam because they lack the amplitude modulation. Hyperbolic metamaterials (HMMs) have recently provided an alternative strategy for building high-performance meta-devices that are capable of flexibly modulating the phase, amplitude and polarization state of light. Here we reveal that both the propagation phase and the Pancharatnam–Berry phase can contribute to the local transmission phase of circularly polarized electromagnetic waves by using HMMs. This thus provides us with great freedom to design HMM units with different cross-sections to independently control the transmission phase and amplitude. Here, we design circularly polarized Airy-beam generators in the microwave and near-infrared domains, which require binary phase and polynary amplitude, and validate the good performance in the microwave experiment. Our work can facilate the generation of a complicated light field that highly requires independent and complete control of the transmission phase and amplitude under circularly polarized incidence.

Keywords: hyperbolic metamaterials, Airy beam, phase and amplitude modulation

PACS: 42.25.Lc, 42.79.−e, 42.30.Lr, 78.67.Pt **DOI:** 10.1088/1674-1056/ab96a1

1. Introduction

As a kind of diffraction-free beams, Airy beams have attracted much attention due to their intriguing self-bending, diffraction-free, and self-healing properties.[1–4] By making use of these unique properties, numerical potential applications have been explored, including light-sheet microscopy,[5,6] optical nano/micromanipulation,[4] optical trapping,[7] optical steering,[8] and curved plasma generation.[9] Customary approaches to generate Airy beams usually require very bulky and complex optical systems, including a spatial light modulator and a Fourier transform lens,[3,4] which is against high-density photonic integration.

Metasurfaces, the two-dimensional version of metamaterials, have served as an innovative platform for manipulating the properties of electromagnetic (EM) waves by locally modulating the phase, amplitude, and/or polarization state of the scattered field in a subwavelength scale.[10–17] Inspired by the flexibility of locally controlling the phase and amplitude of light, metasurfaces have been broadly employed to generate Airy beams for both surface waves at the chip level[18–23] and free-space light.[23–30] The Airy beams for surface waves are revealed with plasmonic metasurfaces.[18–23] For generating the Airy beams for free-space light, both of plasmonic and dielectric metasurfaces are used either for linearly or circularly polarized light incidence.[23–30] However, the Airy beams with plasmonic metasurfaces still face the issue of low transmission efficiency which is defined as the ratio of the maximum electric field intensity of the Airy beams to the intensity of the incident plane waves,[29,31,32] due to the intrinsically low conversion efficiency for plasmonic meta-atoms.[23–29] The Airy beams with dielectric metasurfaces can address the issue of low transmission efficiency, but they typically have a poor quality due to the lack of amplitude modulation.[30] Quite recently, a novel approach for constructing transmissive metasurfaces, with high working efficiencies (the total transmission/incidence ratio) and broad working bands has been established with hyperbolic metamaterials (HMMs).[32–35] HMMs can support a branch of surface waves (SWs) on their lateral walls, and they use SWs propagation inside the HMMs to manipulate the transmission phase and amplitude. HMMs have been demonstrated to be capable of molding the wave-front of the transmitted EM waves in nearly arbitrary ways, leading to a variety of applications such as focusing lenses,[33] polarization manipulation,[34,35] and Airy beam generation for linearly polarized EM waves.[32]

In this paper, it is shown that the local transmission phase of circularly polarized EM waves is associated with both the propagation phase and the Pancharatnam–Berry (PB) phase. The local transmission amplitude of circularly polarized EM waves through the HMM is highly dependent on its cross-sections. Meanwhile, we can always make the local transmission phase reach the pre-designed value by modulating the orientation angle to realize particular wave-manipulation applications. As a demonstration of strategies for obtaining a complex

*Project supported by the National Natural Science Foundation of China (Grant Nos. 11474116 and 11674118).

†Corresponding author. E-mail: chen.lin@mail.hust.edu.cn

EM field, we have designed and fabricated a microwave Airy beam generator, which demonstrated good performance in experiment.

2. Results and discussion

Figure 1 shows the schematic diagram of a circularly polarized Airy beam generator with HMMs, and the HMM meta-atom, comprised of an alternating metal-dielectric multilayer, is presented in the top right corner. The Airy beam generator is assumed to be sufficiently long along the y direction so that the field intensity distributions along the y direction are uniform. Figure 1 merely shows the cross-sectional field intensity distribution of the Airy beam in an arbitrary x–z plane along the y direction. It has been demonstrated that such an HMM array structure can support a branch of SW mode on both lateral walls, whose propagation constant is closely related to the geometry and the gap separation between the adjacent HMM units.[33] A rectangle-shaped HMM (RHMM) can serve as a birefringent optical material (i.e., a phase shift can be introduced between the length and width directions because of different propagation constants of the SW modes). With the definition of the long- and short-edges of RHMM as l and s ($l \geq s$), the modal birefringence can be numerically retrieved by calculating the dispersion relations of l- and s-polarized SW modes with the eigenmode solver of commercial software CST Microwave Studio. As a validation in the microwave regime, the multilayer structure is made up of alternate copper and FR4 layers. For the RHMM array with transversal period $P = P_x = P_y = 13$ mm, longitudinal period $P_z = t_\mathrm{m} + t_\mathrm{d} = 0.518$ mm, and short-edge width $W_s = 6$ mm, the dispersion relations of the SW modes for different W_l are shown in Fig. 2(a). There is no birefringence for $W_l = W_s = 6$ mm as the propagation constants of the l- and s-polarized SW modes are equal (blue solid line in Fig. 2(a)). With the increase of W_l, the dispersion relation of the s-polarized SW mode varies gently, while that of the l-polarized SW mode changes dramatically. Consequently, the birefringent index, defined as the difference of effective refraction index of the l- and s-polarized SW modes, is increased monotonously (Fig. 2(b)).

Considering the modal birefringence of an RHMM unit, we can denote the complex transmission coefficients for l- and s-polarization incidences as

$$t_l = A_l \exp(\mathrm{j}\phi_l), \quad t_s = A_s \exp(\mathrm{j}\phi_s), \tag{1}$$

where A_l and A_s stand for the transmission amplitudes; ϕ_l and ϕ_s represent the transmission phases along the l- and s-polarized directions, respectively. Besides, the orientation angle between the x axis of the laboratory coordinate and the l axis of the RHMM unit is denoted as θ (Fig. 1) Hence, the complex transmission electric field for left circular polarization (LCP) and right circular polarization (RCP) incidences can be expressed as[33]

$$\boldsymbol{E}_t = \frac{1}{2}(t_l + t_s)\boldsymbol{e}_\mathrm{co} + \frac{1}{2}(t_l - t_s)\exp(\sigma \mathrm{j}2\theta)\boldsymbol{e}_\mathrm{cross}, \tag{2}$$

where $\boldsymbol{e}_\mathrm{co}$ and $\boldsymbol{e}_\mathrm{cross}$ are the circular-polarized based vectors for the co-polarized and cross-polarized EM waves, respectively. $\sigma = \pm 1$ is for the LCP ($\sigma = 1$) and RCP ($\sigma = -1$) incident EM waves, respectively. Combining Eqs. (1) and (2) yields the cross-polarized transmission electric field, $\boldsymbol{E}_\mathrm{t,cross}$, as

$$\begin{aligned} \boldsymbol{E}_\mathrm{t,cross} &= \frac{1}{2}\left[A_l \exp(\mathrm{j}\phi_l) - A_s \exp(\mathrm{j}\phi_s)\right] \exp(\mathrm{j}2\sigma\theta)\, \boldsymbol{e}_\mathrm{cross} \\ &= \frac{1}{2} C \exp(\mathrm{j}\chi) \exp(\mathrm{j}2\sigma\theta)\, \boldsymbol{e}_\mathrm{cross}, \end{aligned} \tag{3}$$

where C and χ are the modulus and argument of the complex value $[A_l \exp(\mathrm{j}\phi_l) - A_s \exp(\mathrm{j}\phi_s)]$, respectively. The local transmission amplitude of $\boldsymbol{E}_\mathrm{t,cross}$ is $C/2$, which is merely dependent on the RHMM cross section, and is not affected by the orientation angle θ. As for the local transmission phase of $\boldsymbol{E}_\mathrm{t,cross}$, it is the sum of the propagation phase χ and PB phase $2\sigma\theta$, which are determined by the RHMM cross-section and θ, respectively. We can thus flexibly design the HMMs of different cross-sections and tune their orientation angles to generate a particular complex EM field. To generate Airy beams, it is highly desirable to construct binary phase and polynary amplitude distributions. We can firstly change the long-edge width of the RHMM, W_l, to make the local transmission amplitude of $\boldsymbol{E}_\mathrm{t,cross}$ follow the desired polynary amplitude distributions, regardless of its local transmission phase. Afterwards, we can simply tune θ to change the PB phase to make the transmission phase (the sum of the propagation phase χ and PB phase $2\sigma\theta$) follow the binary phase distributions (i.e., alternative appearing 0 and π phase profile).

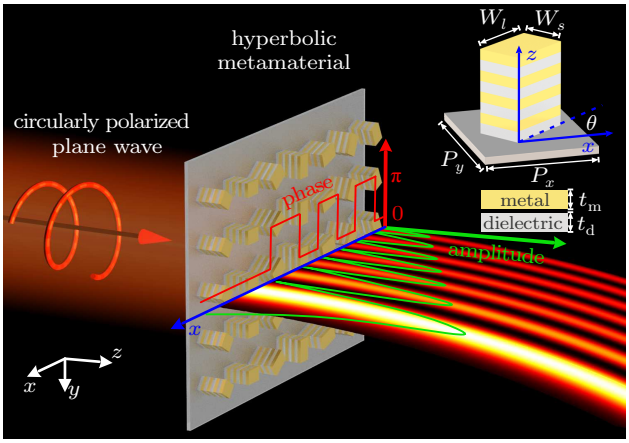

Fig. 1. Schematic diagram of an HMM Airy beam generator, where the HMM meta-atom is presented in the top right corner. The thicknesses of the metal and dielectric layers are denoted by t_m and t_d, respectively. The widths of long- and short-edges of HMM are denoted by W_l and W_s, respectively. The angle between the l axis and the x axis is the orientation angle θ. LCP plane waves normally illuminate the HMM Airy beam generator from the left-hand side.

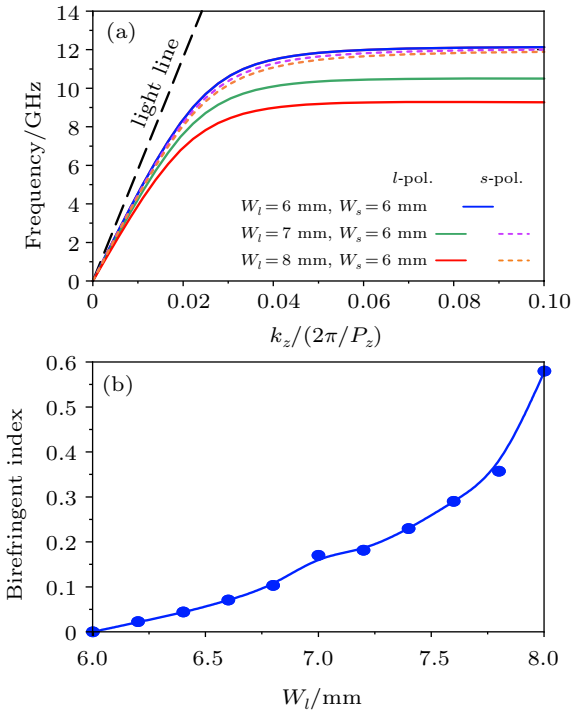

Fig. 2. (a) The dispersion relations of l- and s-polarized fundamental SW modes for RHMM with different W_l. (b) The birefringent index between l- and s-polarized fundamental SW modes as a function of W_l at 8.6 GHz. RHMM meta-atom is made up of multi-layered copper (conductivity of 5.8×10^7 $\Omega^{-1}\cdot$m^{-1} and thickness of $t_m = 0.068$ mm) and FR4 (relative permittivity of 4.3+0.025j and thickness of $t_d = 0.45$ mm).

Using the finite difference time domain (FDTD) method of the commercial software Lumerical FDTD Solutions, we simulated the EM responses of the RHMM arrays. It is emphasized here that both of the LCP and RCP incidences can be used to design the Airy beam generator, we have merely taken the LCP incidence as an example. In this case, both of the LCP and RCP components exist in the output space, but the device's geometrical parameters have been designed to enable the phase and amplitude distributions of the RCP component to follow the Airy envelope. The transmission amplitude and propagation phase of the RCP component vary with W_l (from 6 mm to 8 mm) under LCP incidences at 8.6 GHz, as respectively shown with red squares and blue dots in Fig. 3. For realizing binary phase distributions, the PB phase can be flexibly modulated by θ to make the local transmission phase alternatively appear at the 0 and π phase. Different PB phases are introduced to keep the transmission phase of the RCP component constantly at 0 and π, respectively. The required orientation angle for 0 and π can be extracted as

$$\theta_0 = -\chi/2, \theta_\pi = -(\pi-\chi)/2, \tag{4}$$

where θ and θ_π represent the orientation angles used in Figs. 3(a) and 3(b), respectively.

For the generation of the Airy beam, the transmitted EM waves of an HMM Airy beam generator should satisfy the initial envelope of the Airy beam. For a finite energy 1D Airy beam its electric field distribution satisfies[3]

$$\phi(\xi,s) = \mathrm{Ai}\left[s-\left(\frac{\xi}{2}\right)^2+\mathrm{j}(a\xi)\right] \times \exp\left[as-\left(\frac{a\xi^2}{2}\right)-\mathrm{j}\left(\frac{\xi^3}{12}\right)+\mathrm{j}\left(\frac{a^2\xi}{2}\right)+\mathrm{j}\left(\frac{s\xi}{2}\right)\right], \tag{5}$$

where Ai represents the Airy function, a is the decay factor to obtain the finite energy Airy beam, and $s = (x-x_0)/w$ denotes the normalized dimensionless transverse coordinate. In addition, x, x_0, w, and $\xi = z/(k_0w^2)$, respectively, represent the real laboratory coordinate, the reference coordinate for normalization, the scaling length, and the propagation length normalized with the Rayleigh distance (k is the wavenumber in free space) Apparently under the condition of $\xi = 0$, we can write the initial Airy envelope as

$$\phi(\xi=0,x) = \mathrm{Ai}[(x-x_0)/w]\exp[a(x-x_0)/w]. \tag{6}$$

In the light of the Airy function, $\phi(\xi=0,x)$ must be real values. Namely, the initial phase experiences alternating values of 0 and π.

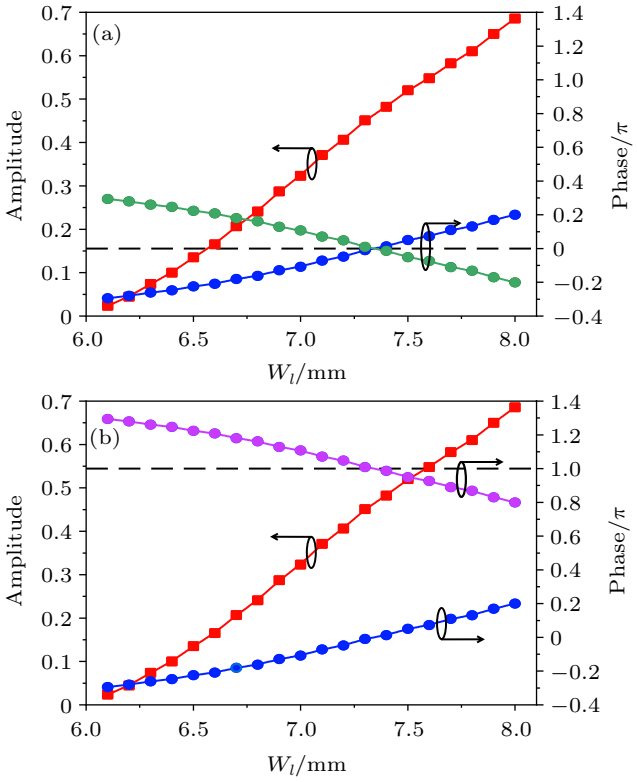

Fig. 3. The amplitude (red line) and propagation phase (blue line) of the transmitted RCP electric field as a function of W_l upon LCP incidences at 8.6 GHz. The introduced PB phase [green line in (a) and purple line in (b)] causes the transmission phase of RCP to be zero [parallel dashed lines in (a)], and to be π [parallel dashed lines in (b)]. 32 pairs of copper/FR4 layers and 2 mm thick FR4 substrate are used for the RHMM meta-atom, while the other geometrical parameters are the same as those in Fig. 2.

For the generation of the 1D Airy beam, we can arrange the RHMM meta-atoms with various lengths of cross-sectional long-edges and orientation angles along the x direction to enable $\boldsymbol{E}_{t,cross}$ to satisfy the initial Airy envelope, while keeping the y direction periodic (shown in Fig. 1). Specifically,

we selected the parameters a, w, and x_0 as 0.01, $P/0.3$, and 513.5 mm, respectively, to design the Airy beam generator. We arranged 50 RHMM meta-atoms along the x direction with equidistant samplings, while keeping uniform along the y direction using 25 RHMM units. Figure 4(a) presents the Airy beam profile, where the solid red line represents the Airy beam profile obtained from Eq. (6) and the blue dots represent the actual sampling points. The corresponding geometric parameters and orientation angles of the RHMM units can be found in Fig. 4(b).

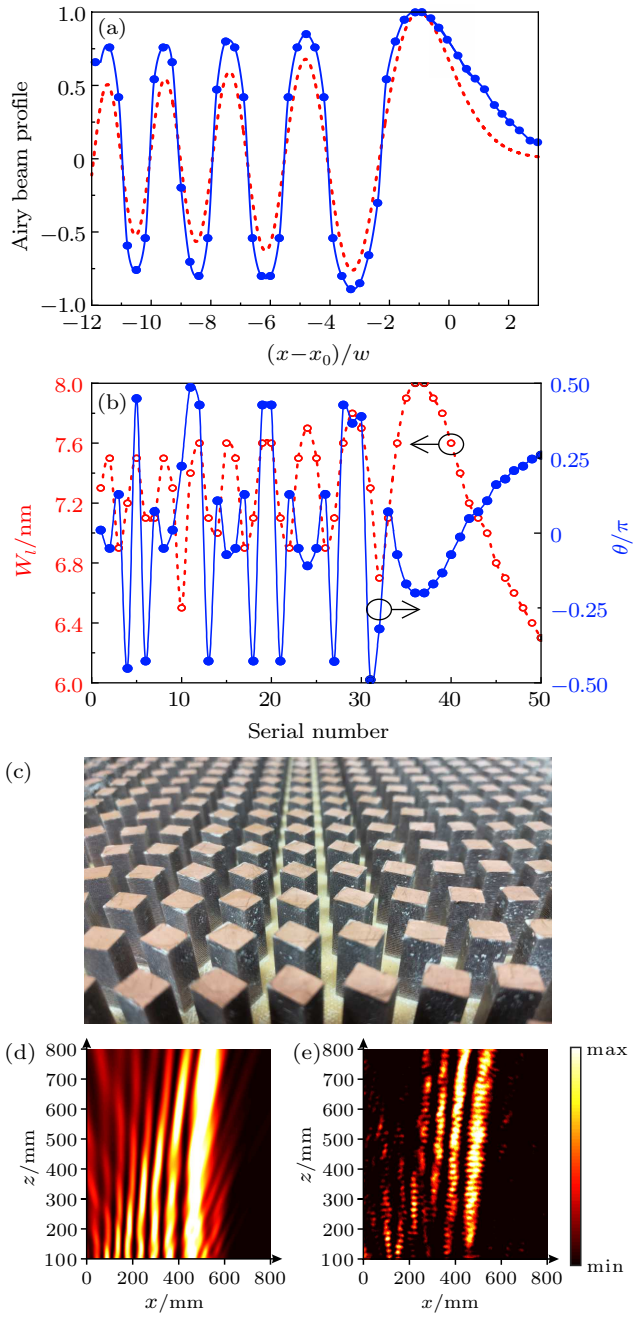

Fig. 4. Design and verification of the HMM Airy beam generator. (a) Airy beam profile: red line for the field envelop of Airy beam extracted by Eq. (6) and blue dots for sampling points. (b) W_l and θ as a function of the serial number of the RHMM unit. (c) A part of the fabricated sample. (d), (e) The electric field intensity distributions of the transmitted RCP waves obtained by FDTD simulation (d), and by near-field scanning experiment (e) at 8.6 GHz.

In the design, the LCP component always co-exists in the output space, but its electric field is always orthogonal to that of the RCP component. Consequently, it does not affect the generated field distributions of the Airy beam that is formed by the RCP component. We performed FDTD simulations to model the EM response of the HMM Airy beam generator and verified the generation of the Airy beam with sample fabrication and measurement. A part of the sample is shown in Fig. 4(c). Standard printed circuit board technology was used to fabricate the multilayered alternating copper/FR4 layers, and the final pattern of the RHMM arrays was formed using a standard mechanical milling technique. In the measurement, the distance between the source and the sample was 2500 mm, and the vector network analyzer was used to acquire the near-field distributions of the complex amplitude of the electric field along the x and y directions, E_x and E_y. The complex amplitude of the electric field of the RCP can thus be extracted by

$$E_{\mathrm{RCP}} = \frac{1}{\sqrt{2}}\left[\mathrm{Re}\left(E_x\right) - \mathrm{Im}\left(E_y\right)\right] + \frac{\mathrm{j}}{\sqrt{2}}\left[\mathrm{Re}\left(E_y\right) + \mathrm{Im}\left(E_x\right)\right]. \tag{7}$$

Figures 4(d) and 4(e) show the simulated and measured field intensity distributions, respectively, at 8.6 GHz, which clearly indicate that Airy beams are generated under LCP incidence. The deviation between the simulated and measured results is mainly caused by the near-field scanning measurement due to the following three main reasons. Firstly, the microwaves illuminating upon the sample are not perfect plane waves because the distance between the sample and the horn antenna is finite. Secondly, owing to the finite size of the sample a small part of the incident waves may go around the sample. Thirdly, the probe and the cable connecting the probe with the vector network analyzer may give rise to a scattering effect.[36,37] The simulated transmission efficiency is 33.2% at 8.6 GHz. Similar to all the transmission-type meta-devices, the HMM Airy beam generators have a transmission efficiency highly dependent on the transmittance of the individual RHMM unit. Restricted by the existing fabrication technology, the maximum width, W_l, of the RHMM unit used in the present work is 8 mm. Our simulated results reveal that the transmission efficiency can be further enhanced if all the used RHMM units have larger widths, which is not shown here. Furthermore, the presented RHMM unit consists of 32 pairs of copper/FR4 layers, associated with a total height of 16.576 mm without the involvement of the substrate. The previous studies on HMM show that the transmittance of the RHMM unit can be increased by increasing the height of the RHMM.[33] As a result, the HMM Airy beam generators with higher transmission efficiencies are highly expectable if the fabrication technology

is improved. In addition, although we have designed and presented the performance of the Airy beam generator at a single frequency of 8.6 GHz, the measured results indicate that it can generate Airy beams within 8.4–8.8 GHz (Fig. 5).

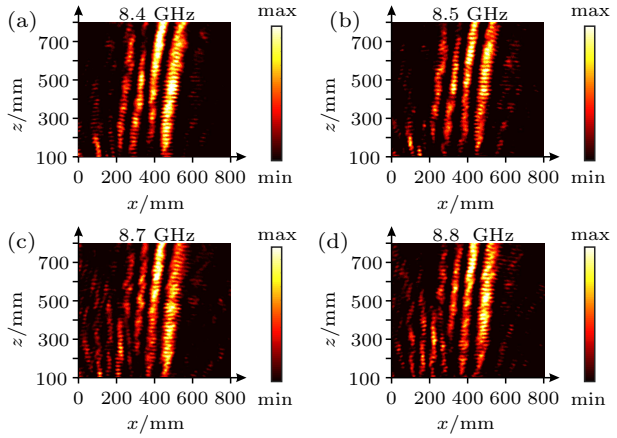

Fig. 5. The measured electric field intensity distributions of the transmitted RCP around the pre-design frequency of 8.6 GHz: (a) 8.4 GHz, (b) 8.5 GHz, (c) 8.7 GHz, and (d) 8.8 GHz.

The design method of a circularly polarized Airy beam generator can also be employed in terahertz and optical frequency domains so long as the proper metal and dielectric materials are used to construct the HMM meta-atoms. Here, we chose to demonstrate a circularly polarized HMM Airy beam generator at 1.55 μm. The RHMM meta-atom, consisting of a silver/silica multilayer, is assumed to deposit on a silica substrate.[38] The thicknesses for each silver and silica layer are $t_m = t_d = 40$ nm, and ten pairs of silver/silica layers are used to construct the RHMM meta-atom. The lattice constants along the x- and y-directions are $P = P_x = P_y = 600$ nm. The RHMM units have a long-edge width varying from 265 nm to 355 nm and a constant short-edge width of 260 nm. The amplitude and propagation phase of the transmitted RCP electric field under LCP incidence are shown in Fig. 6(a). Again, we can modulate the orientation angle to vary the PB phase so that the local transmission phase alternately appears at 0 and π. To experimentally implement the fabrication of such an HMM structure in the optical regime, we can use deposition techniques such as electron beam evaporation or magnetron sputtering deposition to prepare the silver/silica multilayer. The pattern of the RHMM array can be formed by means of etching techniques such as reactive ion etching and focused ion-beam milling. Following the pre-designed HMM presented in Fig. 6(a), we designed an Airy beam generator with $w = P/0.3$ and $x_0 = 23.7$ μm under LCP incidence, with the geometric parameters and orientation angles of the RHMM units as shown in Fig. 6(b). Figure 6(c) shows the simulated electric field intensity distribution of the transmitted RCP waves, suggesting the generation of an Airy beam, with the transmission efficiency of 32.5% at 1550 nm.

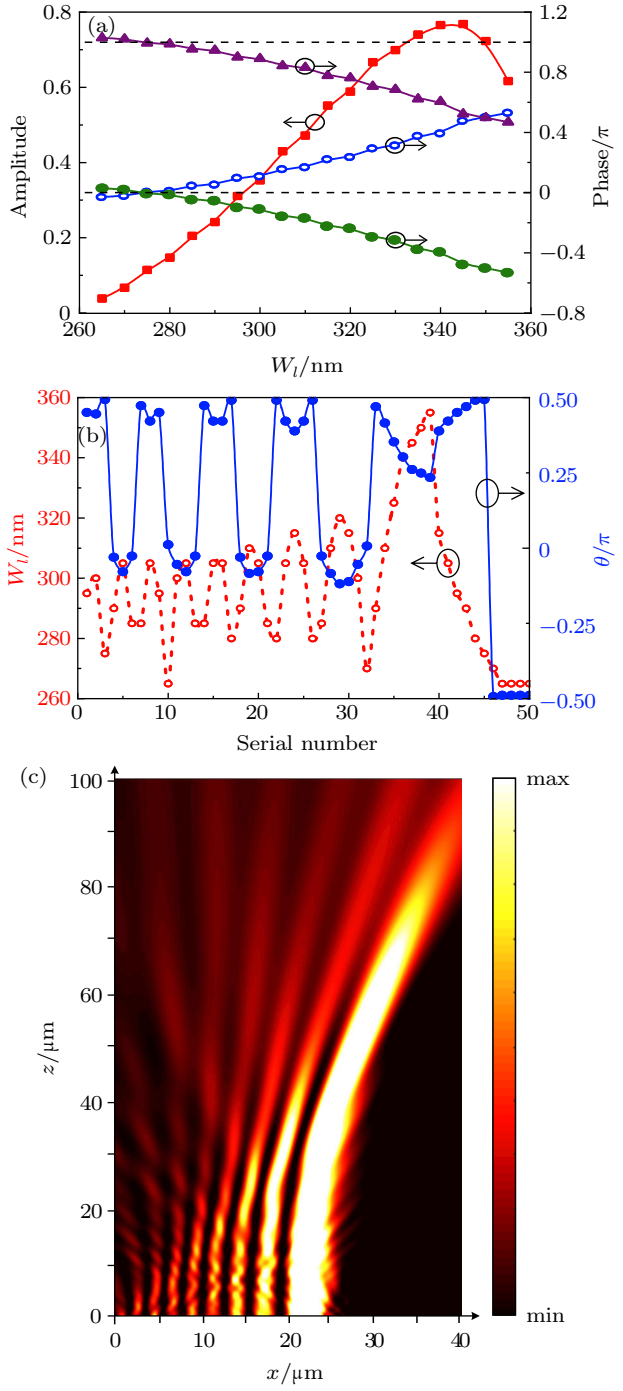

Fig. 6. Numerical demonstration of an HMM Airy beam generator in the near-infrared range. (a) The amplitude (red line) and propagation phase (blue line) of the transmitted RCP electric field as a function of W_l. The introduced PB phases, denoted as green and purple lines, cause the transmission phase of RCP to be zero and π, respectively. (b) W_l and θ as a function of the serial number of the RHMM unit. (c) The electric field intensity distribution of the transmitted RCP waves under LCP incidence at 1.55 μm.

3. Conclusion and perspectives

To summarize, we have put forward a general design strategy for constructing high-efficiency circularly polarized Airy beam generators. In contrast to customary metasurface Airy beam generation strategies, both the propagation phase and PB phase can be used to tune the local transmission phase

of circularly polarized EM waves with HMMs. This allows us to independently control the transmission phase and amplitude by changing the cross-section of the HMM unit and its orientation angle to fully satisfy the binary phase and polynary amplitude distributions required by Airy beams. A proof-of-concept experiment was implemented to demonstrate the generation of Airy beams with HMMs under LCP incidence in the microwave regime. This design strategy can also be employed for terahertz and near-infrared waves by scaling down the geometry. The presented results pave a promising avenue for constructing complex photonic devices that require independent and complete control of the transmission amplitude and phase under circularly polarized incidence.

References

[1] Berry M V and Balazs N L 1979 *Am. J. Phys.* **47** 264
[2] Siviloglou G A and Christodoulides D N 2007 *Opt. Lett.* **32** 979
[3] Siviloglou G A, Broky J, Dogariu A and Christodoulides D N 2007 *Phys. Rev. Lett.* **99** 213901
[4] Baumgartl J, Mazilu M and Dholakia K 2008 *Nat. Photon.* **2** 675
[5] Nylk J, McCluskey K, Preciado M A, Mazilu M, Yang Z, Gunn-Moore F J, Aggarwal S, Tello J A, Ferrier D E K and Dholakia K 2018 *Sci. Adv.* **4** eaar4817
[6] Vettenburg T, Dalgarno H I C, Nylk J, Coll-Lladó C, Ferrier D E K, Čižmár T, Gunn-Moore F J and Dholakia K 2014 *Nat. Methods* **11** 541
[7] Zhang P, Prakash J, Zhang Z, Mills M S, Efremidis N K, Christodoulides D N and Chen Z 2011 *Opt. Lett.* **36** 2883
[8] Chen R H and Hong W Y 2019 *Chin. Phys. B* **28** 54202
[9] Polynkin P, Kolesik M, Moloney J V, Siviloglou G A and Christodoulides D N 2009 *Science* **324** 229
[10] Yu N, Genevet P, Kats M A, Aieta F, Tetienne J P, Capasso F and Gaburro Z 2011 *Science* **334** 333
[11] Liu L, Zhang X, Kenney M, Su X, Xu N, Ouyang C, Shi Y, Han J, Zhang W and Zhang S 2014 *Adv. Mater.* **26** 5031
[12] Yu N, Aieta F, Genevet P, Kats M A, Gaburro Z and Capasso F 2012 *Nano Lett.* **12** 6328
[13] Kong X, Xu J, Mo J J and Liu S 2017 *Front. Optoelectron.* **10** 124
[14] Yang T, Lin H and Jia B 2018 *Front. Optoelectron.* **11** 2
[15] Jia W, Ren P W, Tian Y C and Fan C Z 2019 *Chin. Phys. B* **28** 26102
[16] Xu J, Li R Q, Jiang X P, Wang S Y and Han T C 2019 *Acta Phys. Sin.* **68** 117801 (in Chinese)
[17] Wang Q, Kong X, Yan X, Xu Y, Liu S, Mo J and Liu X 2019 *Chin. Phys. B* **28** 74205
[18] Li L, Li T, Wang S M, Zhang C and Zhu S N 2011 *Phys. Rev. Lett.* **107** 126804
[19] Klein A E, Minovich A, Steinert M, Janunts N, Tünnermann A, Neshev D N, Kivshar Y S and Pertsch T 2012 *Opt. Lett.* **37** 3402
[20] Guan C, Yuan T, Chu R, Shen Y, Zhu Z, Shi J, Li P, Yuan L and Brambilla G 2017 *Opt. Lett.* **42** 563
[21] Minovich A, Klein A E, Janunts N, Pertsch T, Neshev D N and Kivshar Y S 2011 *Phys. Rev. Lett.* **107** 116802
[22] Yin X, Chen L and Li X 2018 *Opt. Express* **26** 23251
[23] Wang S, Wang X and Zhang Y 2017 *Opt. Express* **25** 23589
[24] Li Z, Yao K, Xia F, Shen S, Tian J and Liu Y 2015 *Sci. Rep.* **5** 12423
[25] He J, Wang S, Xie Z, Ye J, Wang X, Kan Q and Zhang Y 2016 *Opt. Lett.* **41** 2787
[26] Ding J, An S, Zheng B and Zhang H 2017 *Adv. Optical Mater.* **5** 1700079
[27] Zhang L, Zhang M and Liang H 2017 *Adv. Optical Mater.* **5** 1700486
[28] Li Z, Cheng H, Liu Z, Chen S and Tian J 2016 *Adv. Optical Mater.* **4** 1230
[29] Song E Y, Lee G Y, Park H, Lee K, Kim J, Hong J, Kim H and Lee B 2017 *Adv. Optical Mater.* **5** 1601028
[30] Fan Q, Wang D, Huo P, Zhang Z, Liang Y and Xu T 2017 *Opt. Express* **25** 9285
[31] Hao W, Deng M, Chen S and Chen L 2019 *Phys. Rev. Appl.* **11** 054012
[32] Li H, Hao W, Yin X, Chen S and Chen L 2019 *Adv. Optical Mater.* **7** 1900493
[33] Yin X, Zhu H, Guo H, Deng M, Xu T, Gong Z, Li X, Hang Z H, Wu C, Li H, Chen S, Zhou L and Chen L 2019 *Laser & Photonics Rev.* **13** 1800081
[34] Li J, Guo H, Xu T, Chen L, Hang Z, Zhou L and Chen S 2019 *Phys. Rev. Appl.* **11** 044042
[35] Zhu H, Yin X, Chen L, Zhu Z and Li X 2015 *Opt. Lett.* **40** 4595
[36] Ding X, Monticone F, Zhang K, Zhang L, Gao D, Buroker S N, de Lustrac A, Wu Q, Qiu C W and Alù A 2015 *Adv. Mater.* **27** 1195
[37] Wang R, Wang B, Gong Z and Ding X 2017 *IEEE Photon. J.* **9** 1
[38] Palik E D 1989 *Handbook of Optical Constants of Solids* (San Diego: Academic Press)